Desalination and Water Treatment
www.deswater.com

doi: 10.5004/dwt.2017.20865

77 (2017) 331–341
May

Facile synthesis of $CaAl_2O_4$ nanoparticles by different fuel approach for Cr(VI) removal: a comparative study

K.V. Brungesh[a,b,c,*], B.M. Nagabhushana[a,*], R. Hari Krishna[a], M.N.K. Harish[b], R.S. Raveendra[d], P.A. Prashantha[d]

[a]*Department of Chemistry, M.S. Ramaiah Institute of Technology, Bangalore 560 054, India, emails: brungesh.kv@gmail.com (K.V. Brungesh), bmnshan@yahoo.com (B.M. Nagabhushana), rhk.chem@gmail.com (R. Hari Krishna)*
[b]*Department of Chemistry, Acharya Institute of Technology, Bangalore-560 090, India, emails: mnkharish11@gmail.com*
[c]*Visveswaraya Technological University, Belagavi 590 014, India*
[d]*Department of Chemistry, Sai Vidya Institute of Technology, Bangalore 560 064, India, emails: raveendrars@gmail.com (R.S. Raveendra), prsnthmysore@gmail.com (P.A. Prashantha)*

Received 25 April 2016; Accepted 24 April 2017

ABSTRACT

The present study is aimed at efficient removal of Cr(VI) ions from aqueous solution by employing $CaAl_2O_4$ nanoparticles. $CaAl_2O_4$ nanoparticles were synthesized by solution combustion method by employing two different fuels: glycine and oxalyl dihydrazide. Powder X-ray diffraction, Fourier transmission infrared spectroscopy, scanning electron microscope, and energy dispersive analysis of X-rays were used to characterize the $CaAl_2O_4$ adsorbent before and after adsorption process. $CaAl_2O_4$ nanoparticles synthesized by glycine as fuel (CAG) exhibited excellent Cr(VI) ions removal compared with $CaAl_2O_4$ nanoparticles obtained by oxalyl dihydrazide as fuel (CAO) from aqueous solution at pH 7. The greater adsorption capacity of CAG compared with CAO can be attributed for the fact that CAG has smaller crystallite size about ~8 nm compared with CAO which has crystallite size about ~19 nm. Both CAG and CAO obey second-order kinetics for Cr(VI) ion removal. Correlation coefficient (R^2 = 0.9328 and 0.9213) and adsorption capacity (48.58 and 11.44 mg/g) were obtained for Freundlich and Langmuir isotherm models, respectively, for CAG and CAO.

Keywords: Cr(VI) ion removal; $CaAl_2O_4$ nanoparticles; Glycine; ODH

1. Introduction

Persistent and non-biodegradable nature of heavy metal ions present in water cause diverse effect on human beings, aquatic lives, and microorganisms above the maximum permissible level [1]. In this regard, strict limitations were imposed on metal discharge. But the contaminant complexity in effluents make the wastewater treatment process more difficult. Therefore, metal remediation from wastewater prior to discharge into waterbodies has acquired great importance in recent past [1–3].

In nature, chromium exists in two oxidation states Cr(III) and Cr(VI). Chromium in +3 oxidation state is less soluble, less mobile, less toxic in aqueous medium, whereas chromium in +6 oxidation state is highly soluble, highly mobile, more toxic, powerful epithelial irritant, and carcinogenic as well. The industries like electronics, electroplating, metallurgical, leather tanning, and wood preservatives [2] uses more chromium salts as raw material and are considered to be the main sources of Cr(VI) ions. At pH < 6.5, $Cr_2O_7^{2-}$ predominates with high oxidation potential, whereas CrO_4^{2-} predominates at pH > 6.5 [3]. Strong exposure to Cr(VI) ions may cause nausea, vomiting, severe diarrhoea, and cancer in the digestive tract and lungs [4]. According to the United states Environmental Protection Agency (USEPA), the maximum permissible limit for Cr(VI) is 0.1 mg/L for inland surface water discharge and 0.05 mg/L for potable water,

* Corresponding author.

respectively [5]. Therefore, the removal of Cr(VI) ions from waterbodies is very important due to its severe toxicity.

The removal of heavy metals from wastewater has been well documented by conventional methods which include membrane separation [6], electrodialysis [7], reverse osmosis [8], chemical precipitation [9], reduction [10], and ion exchange [11]. But most of these methods suffer from disadvantages, such as high operational and capital costs, limited tolerance to pH range, incomplete metal removal, and energy requirements. In quest of the better treatment techniques, liquid-phase adsorption finds a place as one of the most efficient methods for the removal of colour, odour, organic, and inorganic pollutants from industrial effluents to overcome the difficulties in above methods. Hence, adsorption technique is now recognized as an effective, efficient, and economic method for heavy metal wastewater treatment [12,13]. Because, it offers flexibility in design and easy operation and results in high-quality treated effluent. In the past few decades, a wide variety of adsorbent materials has been tested and developed which includes, activated carbon [14], zeolites [15], clay minerals [16], chitosan [17], lignocelluloses [18], natural inorganic minerals [19], functionalized polymers [20], etc. However, most of these adsorbents are either not effective due to, diffusion limitation or the lack of enough active surface sites or have shown problems like high cost, difficulty in separation from wastewater or resulting in generation of secondary wastes. By considering these drawbacks, recently nanoadsorbents such as nanoalumina [21], functionalized carbon nanotubes [22], hydroxyapatite nanoparticles [23], etc, have demonstrated high adsorption efficiency for heavy metal removal.

From the available literature, it is clear that use of $CaAl_2O_4$ nanoparticles as adsorbent for heavy metal removal from aqueous solution is an unexplored territory. Hence the present study is aimed at investigation of $CaAl_2O_4$ nanoparticles as adsorbent for the Cr(VI) ions removal from aqueous solution. Two different fuels, glycine and oxalyl dihydrazide, were used to synthesize $CaAl_2O_4$ nanoparticles by simple solution combustion method. The physicochemical characteristics such as surface morphology, crystallite size, and elemental composition were done by scanning electron microscope (SEM), X-ray diffraction (XRD), EDAX, and Fourier transmission infrared spectroscopy (FTIR), respectively, before and after adsorption studies. The adsorption efficiency of Cr(VI) ions on CAG and CAO nanoparticles were investigated by studying different parameters such as effect of pH, contact time, and adsorbent dosage. Different kinetic models were tested to validate the experimental kinetic data.

2. Materials and methods

2.1. Materials and synthesis method

Calcium nitrate hexahydrate, aluminium nitrate pentahydrate, oxalyldihydrazide, glycine, and 1,5-diphenylcarbazide were purchased from Sigma-Aldrich, India. All other chemical reagents used were of analytical grade without further purification. Solutions of Cr(VI) ions (10 ppm) were freshly prepared by dissolving known amount of $K_2Cr_2O_7$ in 1,000 mL of deionized water. 0.1 M NaOH or 0.1 M HCl were used to maintain the desired pH throughout the experiment.

A stoichiometric amount of calcium nitrate hexahydrate, aluminium nitrate pentahydrate, and oxalyldihydrazine (ODH), redox mixture were dissolved in minimum quantity of distilled water in a petri dish and was introduced into a preheated muffle furnace at 500°C. The solution boiled followed by the dehydration, and at the end of the dehydration process, the reaction mixture burnt with flames with the evolution of gaseous byproducts. The combustion process was over within 5 min and a porous white product ($CaAl_2O_4$) was obtained. The product obtained was collected and used for adsorption studies. Similar procedure was adopted for the preparation of $CaAl_2O_4$ nanoparticles using glycine as fuel. The probable reactions taking place during combustion process are as follows:

$$Ca(NO_3)_2 . 4H_2O + 2\,Al(NO_3)_3 . 9H_2O + 4C_2H_6N_4O_2 = CaAl_2O_4 + 12N_2 + 8CO_2 + 34H_2O$$

$$Ca(NO_3)_2 . 4H_2O + 2\,Al(NO_3)_3 . 9H_2O + 4.4\,C_2H_6NO_2 = CaAl_2O_4 + 7N_2 + 8.8\,CO_2 + 33H_2O$$

2.2. Characterization techniques

The phase formation of $CaAl_2O_4$ nanoparticles was analyzed using a X-ray diffractometer (Bruker D8 advanced with a Cu Kα [1.541 Å] radiation nickel filter). The XRD patterns were observed at room temperature with 2θ degree at a scan rate with step time of 2° per min in the range of 10°–80°. SEM (JEOL JSM 840) was used in order to determine the surface morphology of $CaAl_2O_4$ nanoparticles before and after adsorption of Cr(VI) ions. The elemental composition of the adsorbent was obtained by EDAX analysis before and after adsorption process. FTIR was used to analyze the surface functional groups on the adsorbent. FTIR studies are performed on a Perkin Elmer spectrometer (Spectrum 1000) using KBr pellets.

2.3. Batch adsorption experiments

For each experimental run, 50 mL of 10 ppm Cr(VI) ion solution was taken in 250 mL Erlenmeyer flask containing known amount of $CaAl_2O_4$ nanoparticles was agitated at 250 rpm for 30 min at constant temperature. After predetermined time '*t*' (15, 30, 45, and 60 min), 2 mL of the solution was subjected for centrifugation and the residual Cr(VI) ion concentration in supernatant liquid was analyzed spectrophotometrically by UV–visible spectrophotometer (ELICO-156) at 540 nm using 1,5-diphenylcarbazide as complexing agent. Diphenylcarbazide reacts with Cr(VI) ions in acidic medium to form violet coloured Cr(VI)–diphenylcarbazone complex Eq. (1) [30]:

$$2CrO_4^{2-} + 3H_4L + 8H^+ = Cr(HL)^+_2 + Cr^{3+} + H_2L + 8H_2O \quad (1)$$

where H_4L is 1,5-diphenylcarbazide and H_2L is diphenylcarbazone.

The percentage removal of chromium from aqueous solution was calculated from the following Eq. (2):

$$\%\,\text{removal} = \frac{(C_0 - C_e)}{C_0} \times 100 \quad (2)$$

The amount of Cr(VI) adsorbed at equilibrium q_e (mg/g) was calculated by Eq. (3):

$$q_e = \left(\frac{C_0 - C_e}{m}\right) V \quad (3)$$

where C_0 is the initial Cr(VI) ion concentration (mg/L), C_e is the equilibrium Cr(VI) ion concentration (mg/L), V is the volume of solution (L), and m is the mass of adsorbent (g).

2.4. pH at point zero charge

The point of zero charge (pH_{PZC}) is the pH when the charge on the surface of $CaAl_2O_4$ is zero. The procedure of pH_{PZC} drift method [24] could be described as follows: to a series of 250 mL conical flasks, 50 mL of 0.01 N NaCl was added. Then, the initial solution pH values (say pH initial) were adjusted in range between 2 and 12 with intervals of one using 0.01 N HCl solutions and 0.01 N NaOH. After constant value of $pH_{initial}$ had been reached, 0.010 g of $CaAl_2O_4$ sample was added into each conical flask and caped them immediately. Then, stirred them for 12 h to reach equilibrium. After 12 h, pH of solution was measured noted as pH_{final}. The pH_{PZC} of $CaAl_2O_4$ sample is the point when $pH_{initial} = pH_{final}$.

3. Results and discussion

3.1. X-ray diffraction

Figs. 1(a) and (b) represents the XRD patterns of $CaAl_2O_4$ nanoparticles obtained using glycine and ODH as fuels, respectively. XRD patterns of both CAG and CAO exhibited well-resolved peaks corresponding to all the planes of standard monoclinic $CaAl_2O_4$ (JCPDS 70-0134). The crystallite size is calculated from the full width at half maximum (FWHM (b)) of the diffraction peaks using Debye–Scherer's method [25] using the following equation:

$$d = \frac{k\lambda}{\beta\cos\theta} \quad (4)$$

where 'd' is the average crystalline dimension perpendicular to the reflecting phases, 'λ' is the X-ray wavelength, 'k' is Scherer's constant (0.92), 'β' is the FWHM intensity of a Bragg reflection excluding instrumental broadening, and 'θ' is the Bragg's angle. The calculated average crystallite size of CAG and CAO was found to be 8 and 19 nm, respectively.

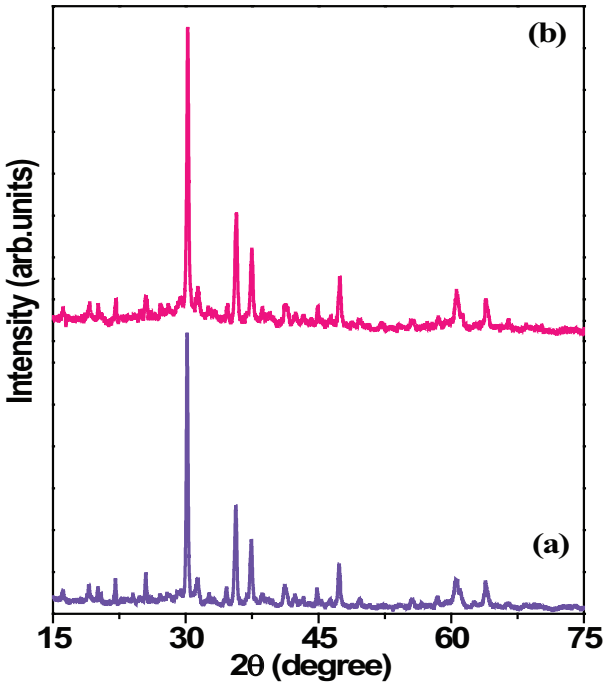

Fig. 1. XRD patterns (a) CAG and (b) CAO nanoparticles.

3.2. Scanning electron micrograph

The scanning electron micrographs and energy dispersive spectra of CAG and CAO nanoparticles before and after adsorption are shown in Figs. 2 and 3, respectively. It is evident from SEM images that there are structural changes on the surface of CAG adsorbent before and after Cr(VI) ion adsorption and are shown in Figs. 2(a) and (b). It is observed that the surface of the adsorbent is porous in nature before adsorption, which were covered by Cr(VI) ions after adsorption indicating the structural changes of CAG adsorbent. Fig. 2(c) shows elemental composition of the adsorbent before treatment and Fig. 2(d) shows EDAX after treatment. It is worth noticing that there appears a Cr peak in samples after treatment which confirms the adsorption of chromium. In addition, the estimated elemental composition such as calcium (Ca), aluminium (Al), and oxygen (O) from the EDAX analysis spectra confirms the composition of $CaAl_2O_4$.

But the surface of CAO particles possess less porous structure (Fig. 3(a)) compared with CAG nanoparticles, therefore, the decreased percentage adsorption of Cr(VI) ions (Fig. 3(b)) is reasonable. Smaller the crystallite size larger is the specific surface area that leads to more number of adsorption active sites, this results in strong interaction between the Cr(VI) ions and adsorbent surface of CAG rather than CAO nanoparticles [26]. EDAX spectra of the CAO samples (Figs. 3(c) and (d)) show similar results as that of CAG and further confirms the Cr(VI) adsorption.

3.3. Fourier transform infrared spectroscopy

The FTIR spectra of CAG and CAO indicated that the broad peaks at 3,487 and 3,465 cm^{-1} (Figs. 4 and 5) shows the presence of stretching and bending vibrations of hydrogen bonded surface –OH groups due to retainment of extra water molecules in addition to metal oxides present within the material [27]. In Fig. 4, the sharp peaks at 1,414 and 1,403 cm^{-1} are due to symmetric stretching vibration of carbonate species which also have been proved by observing a small sharp peak at 880 cm^{-1}. A small peak at 1,642 cm^{-1} corresponds to the deformation vibration of free water molecules, while the sharp peak at 1,412 cm^{-1} was due to the deformation vibration of hydroxyl groups. The peaks at 510 and 550 cm^{-1} correspond to the presence of stretching vibration of Al–O bond (Figs. 4(a) and (b)). This may be due to exposure of Al–O surface area during combustion resulting in the formation of CO_2 and H_2O, which are adsorbed on the surface of Al–O in

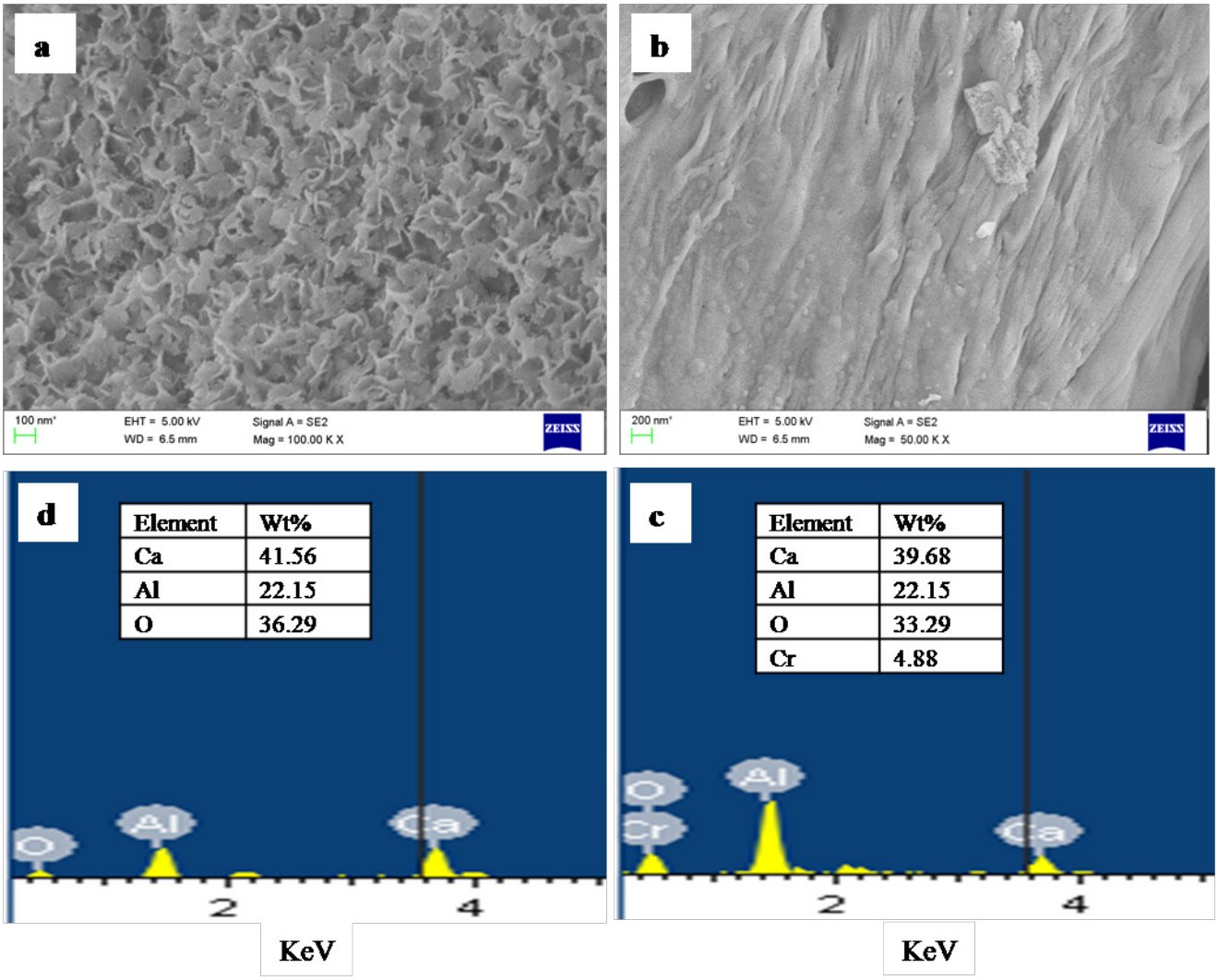

Fig. 2. SEM micrographs of CAG (a) before adsorption and (b) after adsorption; and EDAX spectra of CAG (c) before adsorption and (d) after adsorption.

the form of carbonate and free surface –OH groups [28]. The bands at 783 and 640 cm^{-1} correspond to Al–O bonds at two different spectral range as distinctive in particular [29]. It is attributed that there is no significant amount of water molecules trapped and less number of surface –OH groups present in CAO adsorbent in comparison with CAG nanoparticles leads decreased adsorption of Cr(VI) ions (Fig. 5). The additional peaks observed from ~800 to 1,000 cm^{-1} in both CAG and CAO after treatment confirms the presence of CrO_4^{2-} ions [28] on the surface of the adsorbent ($CaAl_2O_4$).

3.4. Effect of contact time

The effect of contact time on adsorption of Cr(VI) ions on CAG and CAO was studied between 10 and 90 min in order to investigate the equilibrium contact time for maximum adsorption. The 10 ppm Cr(VI) ion solutions were agitated in 250 mL flask at 250 rpm with adsorbent dose of 2 g/L, at neutral pH and the results were shown in Fig. 6. From Fig. 6 it is found that there is a 45% Cr(VI) ion removal efficiency in first 15 min and is increased to 97% at 60 min for CAG, whereas 18% in first 15 min and 47% at 60 min for CAO, respectively. This is because, the increase in contact time increases the diffusion of adsorption sites on adsorbent surface, which leads to more utilization of adsorption sites by Cr(VI) ions [30]. Hence, 60 min was kept as constant contact time for further adsorption studies.

3.5. Effect of pH

pH is considered to be an important parameter which has significant influence in controlling adsorption process. The effect of pH was determined by studying the adsorption of Cr(VI) ions onto CAG and CAO in a pH range of 1–11, at an initial Cr(VI) ion concentration of 10 mg/L with adsorbent dose of 2 g/L at 60 min contact time at 25°C. The effect of pH on Cr(VI) ion uptake on both CAG and CAO adsorbent was shown in Fig. 7. From the results (see Fig. 7), it is clear that the percentage Cr(VI) ion removal efficiency by both CAG and CAO adsorbents increases gradually with increase in pH from 1 to 7 and decreases with further increase in pH.

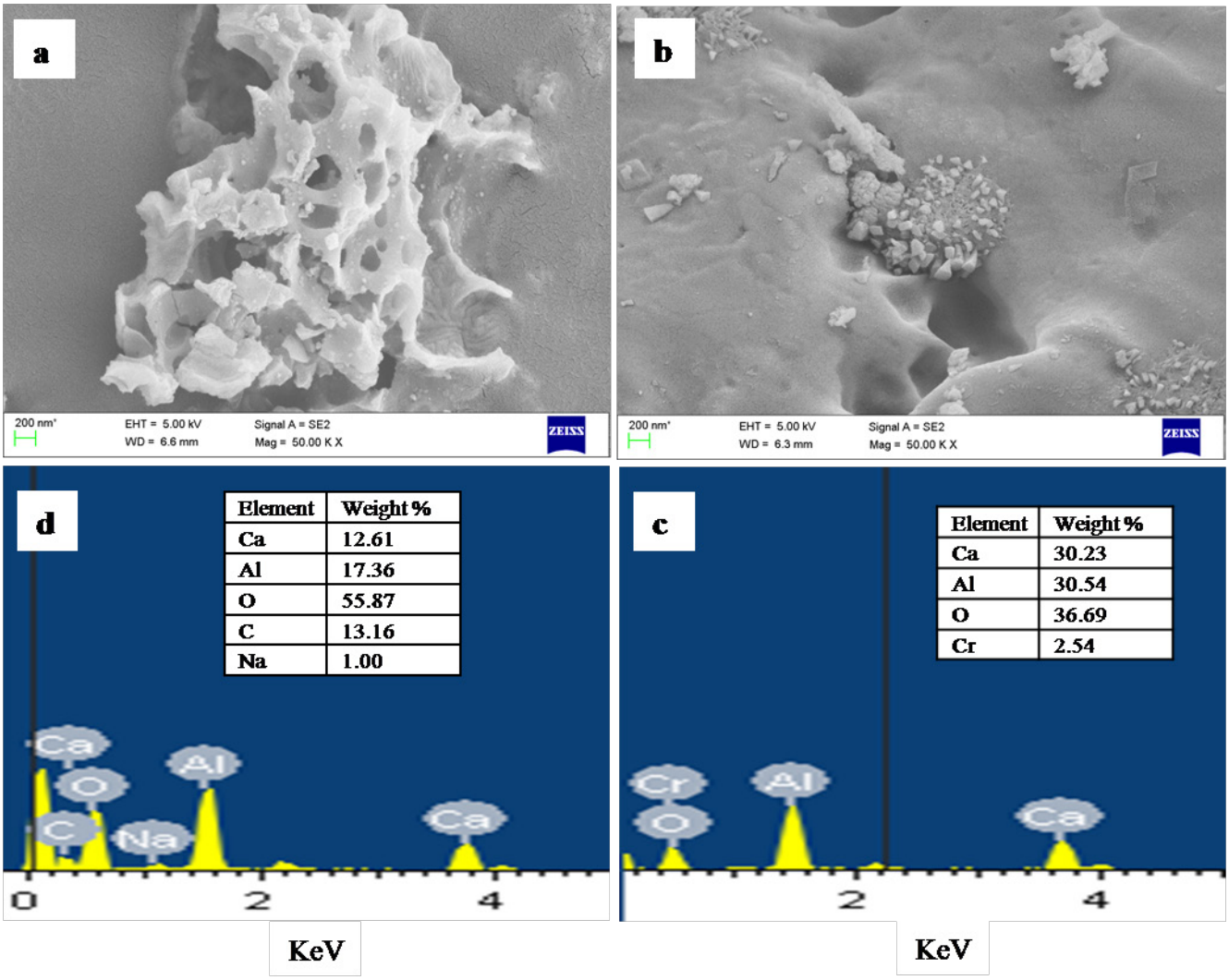

Fig. 3. SEM micrographs of CAO (a) before adsorption and (b) after adsorption; and EDAX spectra of CAO (c) before adsorption and (d) after adsorption.

Bhattacharyya and Gupta [31] reported similar observations for Cr(VI) ions removal using clay as adsorbent. The decrease in adsorption efficiency other than pH 7 may be due to relative lowering of reaction site density in terms of positive charge on the surface. Paul et al. [32] reported similar observation in adsorption of Cr(VI) on nanotitania adsorbent. Therefore, we have carried out other experimental parameters keeping pH 7 as optimum for further experiments. However, other researchers have reported optimum efficiency of Cr(VI) ion removal at lower pH. The reason for higher efficiency in acidic pH was explained as follows. Below pH 7, Cr(VI) predominantly exists in $HCrO_4^-$ and CrO_4^{2-} anionic forms [33]. Therefore, the removal efficiency at this pH range is higher due to Coulombic force of attraction between negatively charged ions and positive surface of the adsorbents [34].

3.6. Effect of adsorbent dose

The performance of Cr(VI) ions (10 mg/L) uptake by CAG and CAO nanoparticles were performed by varying adsorbent dose from 0.4 to 2.8 g/L, and the results were shown in Fig. 8. The percentage removal increases with increase in amount of adsorbent and equilibrium is attained at an adsorbent dose of 2 g/L and there is no considerable removal of Cr(VI) ions thereafter. For 2 g/L adsorbent dose, the maximum Cr(VI) ions removal percentage increases from 44 to 97 and 24 to 47 for CAG and CAO nanoparticles, respectively. The increase in Cr(VI) ion removal percentage could be attributed to the availability of more number of adsorption sites for CAG than CAO.

3.7. Recyclability

The recyclability of adsorbent being an important parameter for assessment and real-time applications. This is important considering the fact that better the recyclable efficiency of an adsorbent the more economically viable it is. The cycling runs for the adsorption of Cr(VI) ions using the $CaAl_2O_4$ nanoparticles prepared by ODH and glycine were performed to evaluate its stability and recyclability. The samples were

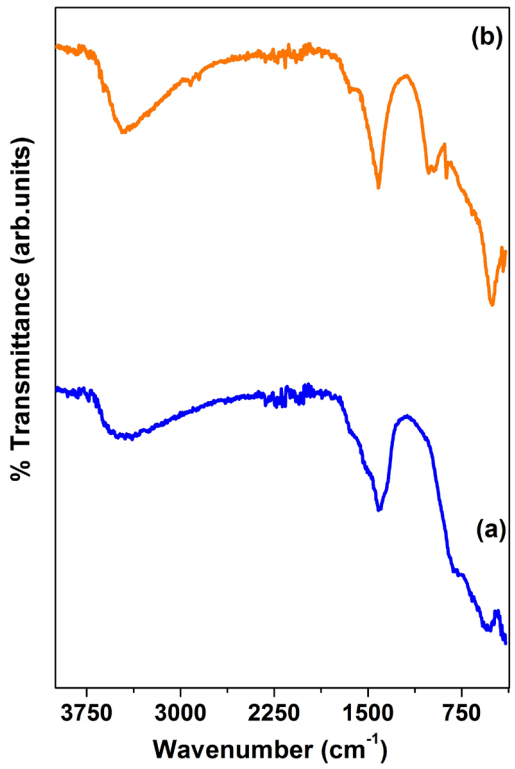

Fig. 4. FTIR spectra for CAG (a) before adsorption and (b) after adsorption.

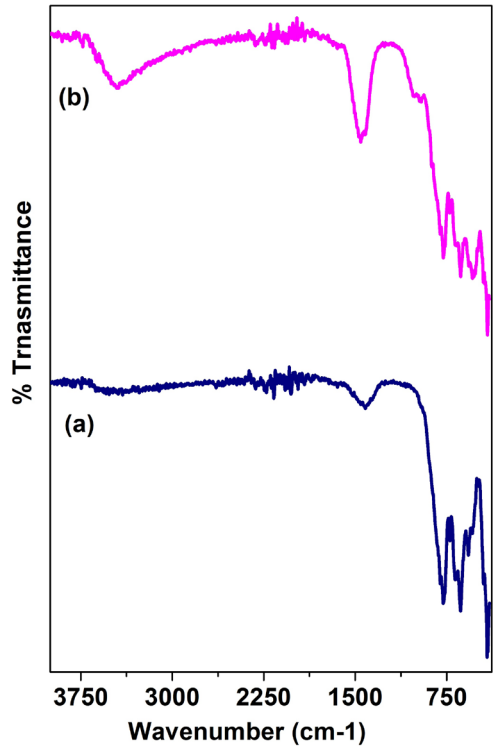

Fig. 5. FTIR spectra for CAO (a) before adsorption and (b) after adsorption.

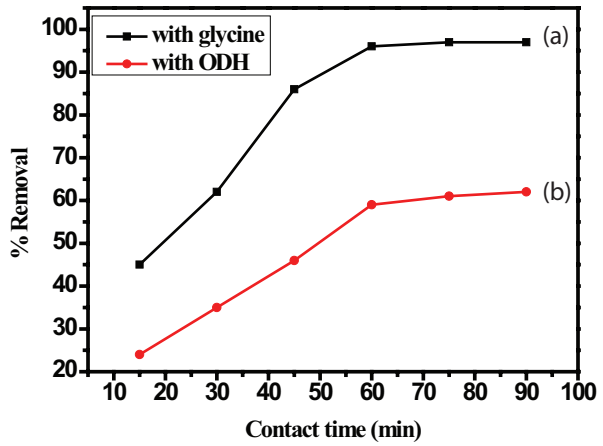

Fig. 6. Effect of contact time on Cr(VI) removal by $CaAl_2O_4$ nanoparticles by (a) glycine and (b) ODH.

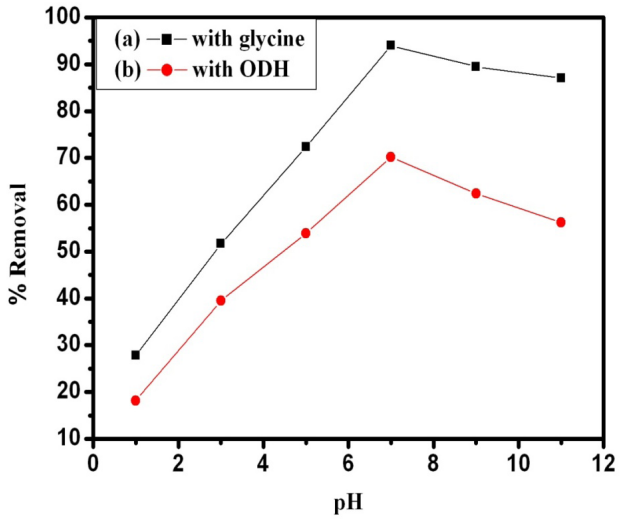

Fig. 7. Influence of pH on Cr(VI) removal by $CaAl_2O_4$ nanoparticles by (a) glycine and (b) ODH.

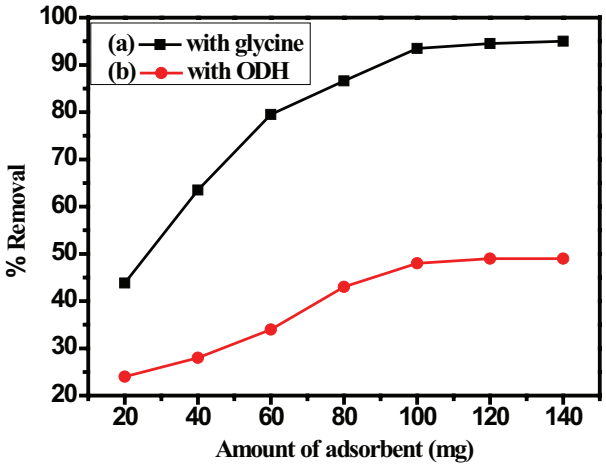

Fig. 8. Effect of adsorbent dose on Cr(VI) removal by $CaAl_2O_4$ nanoparticles by (a) glycine and (b) ODH.

filtered using ashless filter paper, washed with deionized water, and then heated to regenerate the adsorbent and restore the active sites for adsorption. Similar procedure was followed after each cycle and its adsorption studies were carried out by usual batch adsorption techniques. The results of the recycling experiments are presented in Fig. 9. From the results it is clear that up to three cycles there is slight decrease in the adsorption removal of Cr(VI) ions but beyond three cycles there was significant decrease in the removal efficiency. The observed decrease might be due to heating effect during regeneration that leads to decrease in the number of adsorption sites due to decrease in surface area.

3.8. pH at point zero charge determination

The pH_{PZC} results of the experiments performed with the $CaAl_2O_4$ adsorbent, where the pH ranged from 2 to 12. According to Fig. 10, the pH_{PZC} of the CAG and CAO was found to be 7.5 and 7.9, which indicates the near neutral character of the $CaAl_2O_4$ surface, with the below the pH_{PZC} value, the surface of $CaAl_2O_4$ is positively charged due to protonation [35], favouring the adsorption of anions. Above the pH_{PZC}, the $CaAl_2O_4$ surface has a negative charge which favours the adsorption of cation species.

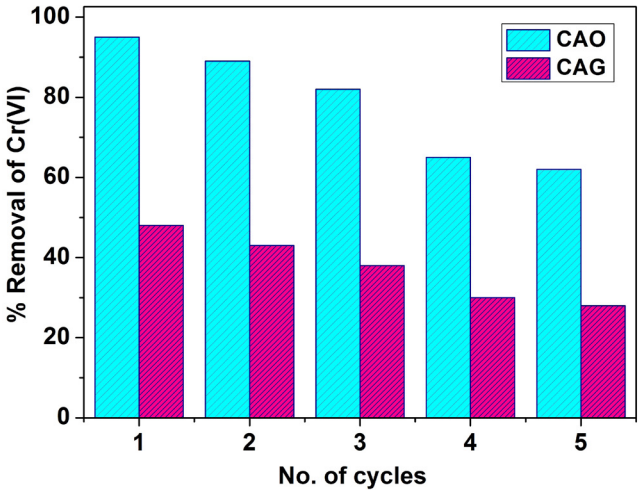

Fig. 9. Percentage removal of Cr(VI) for regenerated adsorbent at different cycle runs.

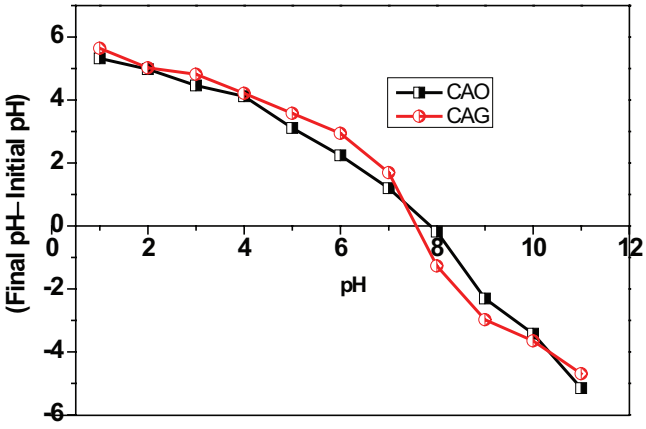

Fig. 10. Point zero charge results of CAO and CAG.

3.9. Mechanism of adsorption

The mechanism of Cr(VI) ion adsorption on the adsorbent surface is usually explained on the basis of surface charges created at specific pH and charge on the ionic species in aqueous solutions [36]. However, in the present case optimum removal was obtained slightly above neutral pH which is greater than the pH_{PZC}. This suggests that the positive surface of the adsorbent favours the adsorption of negatively charged ions (in this case CrO_4^{2-}). Further, the driving force or mechanism of adsorption can also be explained on the basis of Lewis acid sites on the $CaAl_2O_4$. Coster et al. [37] have reported that aluminates behave as Lewis acids and there are two different kinds of Lewis sites in aluminates (i) tetrahedral sites and (ii) pentagonal sites. These Lewis sites can accept the negative charges or have affinity for the negative charges. In this particular case at neutral pH, Cr(VI) ions exists as CrO_4^{2-} as a dominant species. These chromate anions formed get adsorbed to the Lewis sites on the aluminates due to the electrostatic forces. The diagrammatic representation of the mechanism of adsorption is shown in Fig. 11.

4. Isotherm models

Adsorption isotherms are important models in examining the adsorption capacity between adsorbate and adsorbent, and in adsorbent optimization [38]. To investigate equilibrium adsorption capacity of Cr(VI) ions onto CAG and CAO nanoparticles, Langmuir and Freundlich isotherms were employed in the present study.

4.1. Freundlich isotherm

The Freundlich isotherm assumes that the adsorption occurs with stronger binding sites onto a heterogeneous surface in the beginning and decreased binding strength upon increased degree of adsorption sites occupation [39]. The linearized Freundlich equation can be written as:

$$\ln q_e = \ln K_F + \frac{1}{n} \ln C_e \tag{5}$$

where q_e is the amount of chromium adsorbed at equilibrium (mol/g), C_e the equilibrium concentration of chromium in solution (mol/L), K_F the Freundlich constant ((mmol/kg)$^{1-1/n}$) indicative of the relative adsorption capacity and $1/n$ is arbitrary constant related to adsorption intensity. The value of n lies in between 1 and 10 is indicative of favourable adsorption. A plot of Freundlich isotherm, $\ln(q_e)$ vs. $\ln(C_e)$ would give a straight line from which K and n values can be calculated from intercept and slope, respectively (Fig. 12). The values of n for CAG and CAO nanoparticles were found to be 2.9979 and 0.4129, respectively (Table 1), suggesting that adsorption of Cr(VI) ions is favourable for CAG than CAO. This may be attributed due to formation of relatively stronger bonds between Cr(VI) ions on active sites of CAG than CAO nanoparticles.

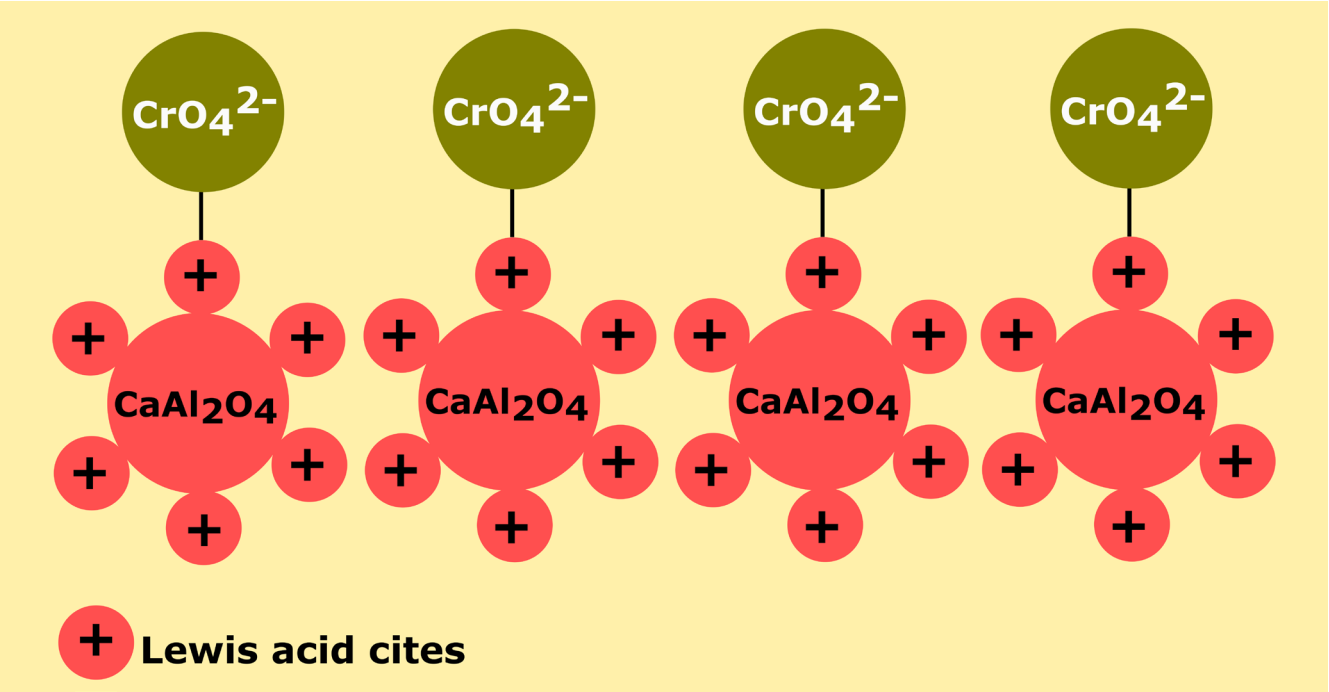

Fig.11. Proposed mechanism for the adsorption of Cr(VI) on to the $CaAl_2O_4$.

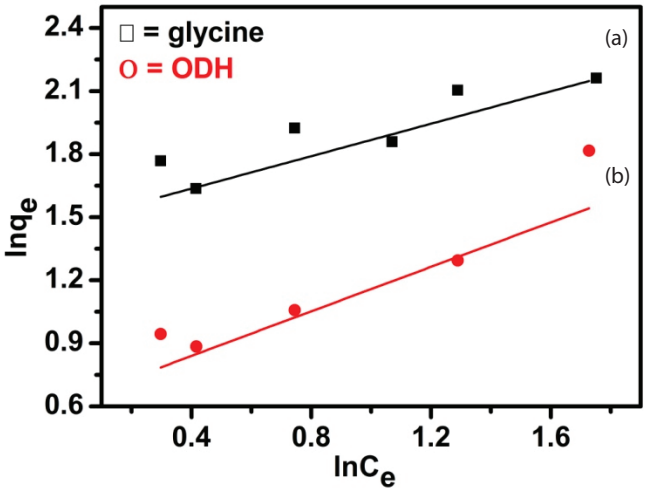

Fig. 12. Linearized Freundlich isotherm for Cr(VI) uptake on $CaAl_2O_4$ nanoparticles by (a) glycine and (b) ODH.

The relative higher R^2 values of Freundlich plot than Langmuir isotherm suggest that the equilibrium adsorption of Cr(VI) ions onto CAG nanoparticles could be best described with the Freundlich isotherm.

4.2. Langmuir isotherm

Langmuir isotherm is the most frequently used model to examine the sorption of pollutant from aqueous solution onto an adsorbent [40]. This model is introduced based on the assumption of adsorption homogeneity over the adsorbent surface. This model is valid for monolayer adsorption

Table 1
Isotherm parameters for adsorption of Cr(VI) on $CaAl_2O_4$ nanoparticles at room temperature

Freundlich isotherm				
Parameters	$1/n$	n	K_F (mg/g)	R^2
CAG	0.3335	2.9979	48.58	0.9328
CAO	2.4218	0.4129	0.0005	0.8126
Langmuir isotherm				
Parameters	q_{max} (mg/g)	K_L (L/mg)	R_L	R^2
CAG	11.4416	1.041	0.0892	0.9213
CAO	0.5145	0.0992	0.1539	0.5726

with a finite number of identical sites [41]. The linear form of Langmuir equation may be written as:

$$\frac{C_e}{q_e}=\frac{1}{K_L\times q_{max}}+\frac{C_e}{q_{max}} \quad (6)$$

where q_e is the amount of chromium adsorbed per unit weight of adsorbent (mg/g), C_e is the equilibrium concentration of Cr(VI) ions in the bulk solution (mg/L), q_{max} is the maximum adsorption capacity, and K_L is the Langmuir constant (L/mg) related to the adsorption. The essential characteristics of a Langmuir isotherm can be expressed in terms of a dimensionless constant separation factor or equilibrium parameter, R_L, which is defined by the following Eq. (7):

$$R_L=\frac{1}{1+(q_{max}\times K_L)C_o} \quad (7)$$

where C_0 is the initial concentration and R_L indicates the shape of the isotherm ($R_L > 1$ unfavourable; $R_L = 1$ linear; $0 < R_L < 1$ favourable, and $R_L = 0$ irreversible). Therefore, adsorption is better if R_L value lies in between 0 and 1. In the present study, the R_L values were 0.0892 and 0.1539 for CAG and CAO, respectively (Table 1), indicating that adsorption is favourable for both the adsorbents.

A plot of C_e/q_e vs. C_e (Fig. 13) gives linearized Langmuir isotherm to calculate the adsorption coefficients. The adsorption capacities, q_{max} for CAG and CAO nanoparticles were 11.44 and 0.5145 mg/g, respectively, and the corresponding correlation coefficient (K_L) values for CAG and CAO were 1.041 and 0.0992 L/mg in the same order. The R^2 values (Table 1) suggests that CAG obeys the Langmuir isotherm better than CAO nanoparticles.

5. Adsorption kinetics

The pseudo-first-order and pseudo-second-order kinetic models were used to determine the rate of adsorption process of Cr(VI) ions on CAG and CAO nanoparticles.

Lagergren [42] proposed a method for adsorption analysis which is the pseudo-first-order kinetic equation in the form:

$$\frac{dq_t}{dt} = k_1(q_e - q_t) \tag{8}$$

where q_e and q_t are the amounts (mg/g) of adsorbate at equilibrium and at time t (min), respectively; and k_1 is the pseudo-first-order rate constant (1/min).

Integration of Eq. (8) at the boundary, $q_t = 0$ at $t = 0$ and $q_t = q_t$ at $t = t$, gives (Eq. (9)):

$$\log\left(1 - \frac{q_t}{q_e}\right) = -\left(\frac{k_1}{2.303}\right)t \tag{9}$$

The linear plot of log ($q_e - q_t$) against time allows one to obtain the rate constant. The pseudo-first-order rate constants for the present study were calculated from the intercept and slope shown in Fig. 14 and found to be non-linear and is not in agreement with correlation coefficient for CAG and CAO nanoparticles. The values k_1 and q_e were shown in Table 2.

The pseudo-second-order kinetic model [43] can be represented in the following form (Eq. 10):

$$\frac{dq_t}{dt} = k_2(q_e - q_t)^2 \tag{10}$$

where k_2 is the rate constant (g/mg min). Integration of Eq. (10) at the boundary, $q_t = 0$ at $t = 0$ and $q_t = q_t$ at $t = t$ and then rearrangement to a linear form gives (Eq. (11)):

$$\frac{1}{q_t} = \frac{1}{k_2 q_e^2} + \frac{1}{q_e}t \tag{11}$$

The value of k_2 and q_e can be determined from the slope and intercept of the plot t/q_t vs. t (Fig. 15). The calculated R^2 value for pseudo-second-order kinetic model is shown in Table 2.

From Table 2, the calculated R^2 values are in good agreement for pseudo-second-order kinetic model. Therefore,

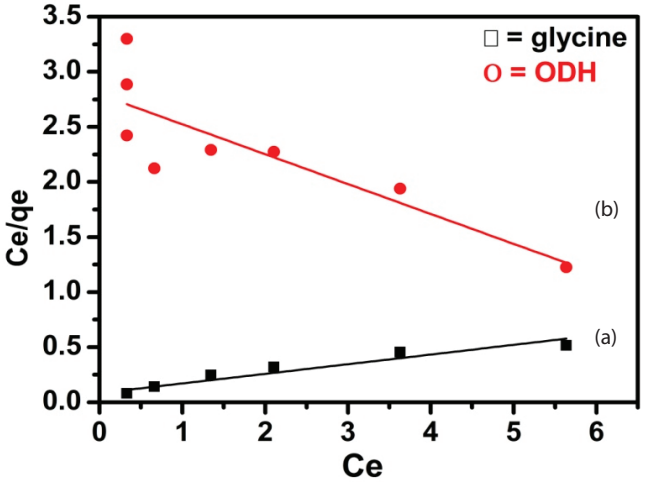

Fig. 13. Linearized Langmuir isotherm for Cr(VI) uptake on $CaAl_2O_4$ nanoparticles by (a) glycine and (b) ODH.

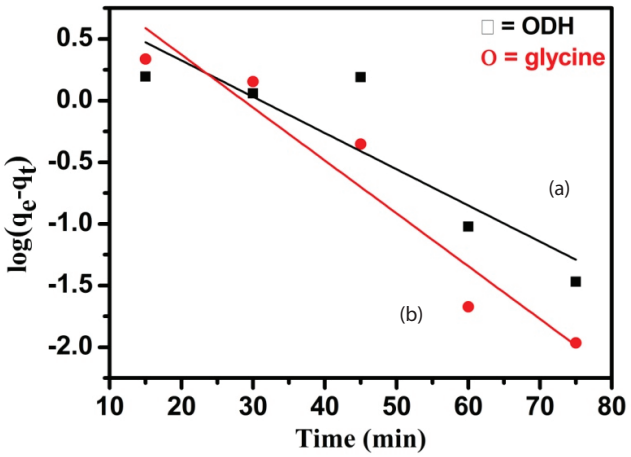

Fig. 14. Pseudo-first-order kinetics of $CaAl_2O_4$ nanoparticles by (a) glycine and (b) ODH.

Table 2
Pseudo-first-order and pseudo-second–order rate constants for adsorption of Cr(VI) on $CaAl_2O_4$ nanoparticles at room temperature

Pseudo-first-order kinetics			
C_0 (mg/L)	k_1(min^{-1})	q_e(mg/g)	R^2
CAG	6.89	27.46	0.7276
CAO	9.27	23.31	0.8993
Pseudo-second-order kinetics			
C_0 (mg/L)	k_2 (min^{-1})	q_e(mg/g)	R^2
CAG	0.0017	26.27	0.9801
CAO	0.0015	25.12	0.9640

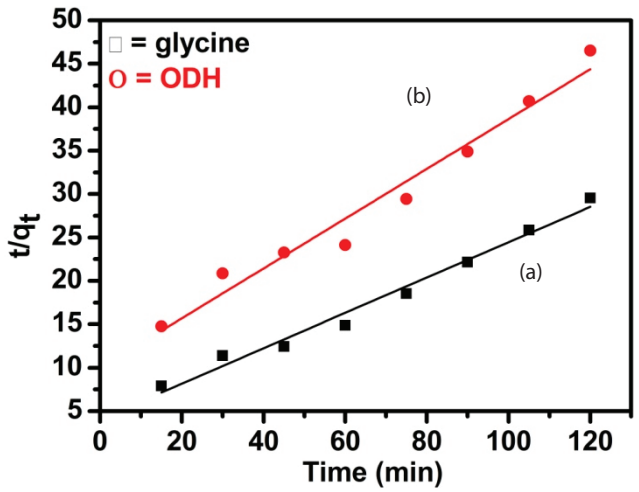

Fig. 15. Pseudo-second-order kinetics of $CaAl_2O_4$ nanoparticles by (a) glycine and (b) ODH.

the adsorption process follows pseudo-second-order kinetic model for Cr(VI) ions adsorption on CAG and CAO nanoparticles.

6. Conclusions

In this study we show that single experimental parameter namely the fuel used in combustion synthesis for preparing adsorbent ($CaAl_2O_4$) plays significant role in the efficient adsorption of Cr(VI) from aqueous solutions. $CaAl_2O_4$ prepared using glycine as fuel exhibits better Cr(VI) removal than the one prepared using ODH. Adsorption of Cr(VI) is highly pH dependent and irrespective of the fuel used $CaAl_2O_4$ showed maximum removal at neutral pH. The surface charge on the $CaAl_2O_4$ was evaluated from pH_{PZC} and probable adsorption mechanism was proposed based on the PZC and Lewis acid–base concept. Lewis acid sites on the $CaAl_2O_4$ is the driving force for the adsorption of Cr(VI) from aqueous solutions. The $CaAl_2O_4$ can be readily recycled and reused up to three cycles without significant loss in its adsorption efficiency. This work demonstrates that the adsorption property of the nanoadsorbents prepared from combustion method can be tuned by fuel selection.

Acknowledgement

The author K.V. Brungesh thanks the principal and management of Acharya Institute of Technology, Bengaluru, for their constant encouragement.

References

[1] V.K. Gupta, I. Ali, Removal of lead and chromium from wastewater using bagasse fly ash—a sugar industry waste, J. Colloid Interface Sci., 271 (2004) 321–328.
[2] A.K. Giri, R. Patel, S. Mandal, Removal of Cr (VI) from aqueous solution by *Eichhornia crassipes* root biomass derived activated carbon, Chem. Eng. J., 185 (2012) 71–81.
[3] J. Kotas, Z. Stasicka, Chromium occurrence in the environment and methods of its Speciation, Environ. Pollut., 107 (2000) 263–283.
[4] K. Mohanty, M. Jha, B.C. Meikap, M.N. Biswas, Removal of chromium (VI) from dilute aqueous solutions by activated carbon developed from *Terminalia arjuna* nuts activated with zinc chloride, Chem. Eng. Sci., 11 (2005) 3049–3059.
[5] EPA, Environmental Protection AGENCY, Environmental pollution control, Alternatives, EPA/625/5-90, EPA 625/4-89/023, Cincinnati: US 1990, Ref-2-Indian Standard, Drinking Water-Specification (1st revision) IS 10500, 1991.
[6] I. Korus, K. Loska, Removal of Cr(III) and Cr(VI)ions from aqueous solutions by means of polyelectrolyte enhanced ultrafiltration, Desalination, 247 (2009) 390–395.
[7] S.K. Nataraj, K.M. Hosamani, T.M. Aminabhavi, Potential application of an electrodialysis pilot plant containing ion-exchange membranes in chromium removal, Desalination, 217 (2007) 181–190.
[8] A. Hafez, S. El-Manharawy, Design and performance of the two-stage/two-pass RO membrane system for chromium removal from tannery wastewater, Part 3, Desalination, 165 (2004) 141–151.
[9] S. Vasudevan, J. Lakshmi, G. Sozhan, Studies on the Al-Zn-In alloy as anode material for the removal of chromium from drinking water in electrocoagulation process, Desalination, 275 (2012) 260–268.
[10] F. Magalhaes, M.C. Pereira, J.D. Fabris, S.E.C. Bottrel, M.T.C. Sansiviero, A. Amaya, N. Tancredi, R.M. Lago, Novel highly reactive and regenerable carbon/iron composites prepared from tar and hematite for the reduction of Cr(VI) contaminant, J. Hazard. Mater., 165 (2009) 1016–1022.
[11] A. Dabrowski, Z. Hubicki, P. Podkoscielny, E. Robens, Selective removal of the heavy metal ions from waters and industrial wastewaters by ion-exchange method, Chemosphere, 56 (2004) 91–106.
[12] V.K. Gupta, P.J.M. Carrott, M.M.L. Ribeiro Carrott, Suhas, Low-cost adsorbents: growing approach to wastewater treatment—a review, Environ. Sci. Technol., 39 (2009) 783–842.
[13] I. Ali, V.K. Gupta, Advances in water treatment by adsorption technology. Nat. Protoc., 1 (2006) 2661–2667.
[14] X. Huang, N. Gao, Z. Hang, Thermodynamics and kinetics of cadmium adsorption onto oxidized granular activated carbon, J. Environ. Sci., 19 (2007) 1287–1292.
[15] M.R. Panuccio, A. Sorgonà, M. Rizzo, G. Cacco, Cadmium adsorption on vermiculite, Zeolite and pumice: batch experimental studies, J. Environ. Manage., 90 (2009) 364–374.
[16] J. Hizal, R. Apak, Modeling of cadmium (II) adsorption on kaolinite-based clays in the absence and presence of humic acid, Appl. Clay Sci., 32 (2006) 232–244.
[17] J.T. Bamgbose, S. Adewuyi, O. Bamgbose, A.A. Adetoye, Adsorption kinetics of cadmium and lead by chitosan, Afr. J. Biotech., 9 (2010) 2560–2565.
[18] E.W. Shin, K.G. Karthikeyan, M.A. Tshabalala, Adsorption mechanism of cadmium on juniper bark and wood, Bioresour. Technol., 98 (2007) 588–594.
[19] K. Sevgi, Adsorption of Cd(II), Cr(III) and Mn(II) on natural sepiolite, Desalination, 244 (2009) 24–30.
[20] G.C. Panda, S.K. Das, A.K. Guha, Biosorption of cadmium and nickel by functionalized husk of *Lathyrus sativus*, Colloid Surf., B, 62 (2008) 173–179.
[21] V. Srivastava, C.H. Weng, V.K. Singh, Y.C. Sharma, Adsorption of nickel ions from aqueous solutions by nano alumina: kinetic, mass transfer, and equilibrium studies, J. Chem. Eng. Data, 56 (2011) 1414–1422.
[22] V.K. Gupta, S. Agarwal, T.A. Saleh, Synthesis and characterization of alumina-coated carbon nanotubes and their application for lead removal, J. Hazard. Mater., 185 (2011) 17–23.
[23] Y. Feng, J.L. Gong, G.M. Zeng, Q.Y. Niu, H.Y. Zhang, C.G. Niu, J.H. Deng, M. Yan, Adsorption of Cd (II) and Zn (II) from aqueous solutions using magnetic hydroxyapatite nanoparticles as adsorbents, Chem. Eng. J., 162 (2010) 487–494.
[24] M.V. Lopez-Ramon, F. Stoeckli, C. Moreno-Castilla, F. Carrasco-Marin, On the characterization of acidic and basic surface sites on carbons by various techniques, Carbon, 37 (1999) 1215–1221.

[25] H.P. Klug, L.E. Alexander, X-Ray Diffraction Procedures for Polycrystalline and Amorphous Materials, John Wiley and Sons, Inc., New York, 1954, p. 716.
[26] B. Cheng, Y. Le, W.Q. Cai, J.G. Yu, Synthesis of hierarchical $Ni(OH)_2$ and NiO nanosheets and their adsorption kinetics and isotherms to Congo Red in water, J. Hazard. Mater., 185 (2011) 889–897.
[27] M. Davis, Infrared Spectroscopy and Molecular Structure, Elsevier Publishing Co., Amsterdam, 1963, p. 318.
[28] Y.E. Kitaev, T.I. Maksimova, K. Hermanowicz, M. Maczka, J. Hanuza, Temperature dependence of IR absorption spectra of the $K_3Na(CrO_4)_2$ Ferroelastic, Phys. Solid State, 55 (2013) 145–149.
[29] R. Hari Krishna, B.M. Nagabhushana, B.N. Sherikar, N. Suriya Murthy, C. Shivakumara, T. Thomas, Luminescence enhancement in monoclinic $CaAl_2O_4$: Eu^{2+}, Cr^{3+} nanophosphor by fuel-blend combustion synthesis, Chem. Eng. J., 267 (2015) 317–323.
[30] R.J. Bhargavi, U. Maheshwari, S. Gupta, Synthesis and use of alumina nanoparticles as an adsorbent for the removal of Zn (II) and CBG dye from wastewater, Int. J. Ind. Chem., 6 (2015) 31–41.
[31] G.K. Bhattacharyya, S.S. Gupta, Adsorption of chromium(VI) from water by clays, Ind. Eng. Chem. Res., 45 (2006) 7232–7240.
[32] M.L. Paul, J. Samuel, R. Roy, N. Chandrasekaran, A. Mukherjee, Studies on Cr(VI)removal from aqueous solutions by nanotitania under visible light and dark conditions, Bull. Mater. Sci., 38 (2015) 393–400.
[33] J.K. Yang, S.M. Lee, Removal of Cr(VI) and humic acid by using TiO_2 photocatalysis, Chemosphere, 63 (2006) 1677–1684.
[34] M.L. Paul, J. Samuel, S. Bedatrayee Das, S. Swaroop, N. Chandrasekaran, A. Mukherjee, Studies on Cr(VI) removal from aqueous solutions by nanoalumina, Ind. Eng. Chem. Res., 51 (2012) 15242–15250.
[35] H.W. Ng, L.Y. Lee, W.L. Chan, S. Gan, N. Chemmangattuvalappil, *Luffa acutangula* peel as an effective natural biosorbent for malachite green removal in aqueous media: equilibrium, kinetic and thermodynamic investigations, Desal. Wat. Treat., 57 (2016) 7302–7311.
[36] N. Dwivedi, C. Balomajumder, P. Mondal, Comparative investigation on the removal of cyanide from aqueous solution using two different bioadsorbents, Water Resour. Ind., 15 (2016) 28–40.
[37] D. Coster, A.L. Biumenfeld, J.J. Fripiat, Lewis acid sites and surface aluminum in aluminas and zeolites: a high-resolution NMR study, J. Phys. Chem., 98 (1994) 6201–6211.
[38] I.A.W. Tan, B.H. Hameed, A.L. Ahmad, Equilibrium and kinetic studies on basic dye adsorption by oil palm fibre activated carbon, Chem. Eng. J., 127 (2007) 111–119.
[39] H.M.F. Freundlich, Uber dye adsorption in losungen, J. Phys. Chem., 57 (1906) 385–470.
[40] I. Langmuir, The constitution and fundamental properties of solids and liquids, J. Am. Chem. Soc., 38 (1916) 2221–2295.
[41] S.D. Khattri, M.K. Singh, Removal of malachite green from dye wastewater using neem sawdust by adsorption, J. Hazard. Mater., 167 (2009) 1089–1094.
[42] S. Lagergren, Zurtheorie der sogenannten adsorption geloesterstoffe. K. Sven. Vetensk.akad. Handl., 24 (1898) 1–39.
[43] Y.S. Ho, G. McKay, Pseudo-second-order model for sorption processes, Process Biochem., 34 (1999) 451–465.